EFFECT OF THERMAL CYCLING ON SUBSEQUENT DROP BEHAVIOR OF CGA1272 ASSEMBLIES

Reza Ghaffarian, Ph.D.
Jet Propulsion Laboratory, California Institute of Technology
Pasadena, CA, USA
reza.ghaffarian@jpl.nasa.gov

ABSTRACT
Ceramic column grid arrays (CGAs) are commercial-off-the-shelf (COTS) area array packaging technologies that are now widely used in numerous high-reliability application electronic systems. In the past, there was always a ceramic version of a plastic package, including the plastic BGA (PBGA) which has the analogous CBGA and CGA. Today, there are few, if any, ceramic (high reliability) versions of the latest technologies. Therefore, the choice of daisy-chain CGAs for solder joint reliability evaluation has become scarce. The daisy-chain package is needed to perform solder-joint reliability under thermal cycling conditions that have now become an integral part of the electronic packaging equation for overall reliability risk analysis. Extensive work has been carried out on this subject within the last two decades by industry.

However, there is limited test data presented in literature on the synergistic effects of sequential thermal cycles and mechanical vibration. In fact, there are none to the author's knowledge on the synergistic effect of thermal cycle and drop shock performance, especially for higher than 1,000 column CGAs. This paper presents the effect of a priori thermal cycle on subsequent drop to failure behavior of CGAs with 1272 columns. After successful assembly of these CGAs onto printed circuit boards (PCBs), they were subjected to two thermal cycle regimes. Three samples were subjected to thermal cycling in the range of –55°/125°C for 300, 400, and 500 cycles and one was subjected to –55°/100°C for 500 cycles. Drop tests were performed first from a height of 36''and then increased to 48''. This paper presents optical and SEM images showing solder damage progression with thermal cycling and optical/ SEM images showing failure mechanisms of CGA1272 assemblies after drop testing with additional thermal cycling.

Key words: Column grid array, CGA, thermal cycle, drop test, combined drop and thermal cycle, extreme cold cycle, Miner's rule, reliability analysis

INTRODUCTION
Single-chip microelectronic packaging technologies can be categorized into three key technologies: (1) PBGAs/LGAs/QFN, (2) CBGAs/CGAs, and (3) smaller foot print chip-scale packages (CSPs) and wafer level packages (WLPs) [1-3]. There are numerous variations of packages in each category, but only CGA categories are discussed in this paper.

For high reliability applications, surface mount leaded packages, such as ceramic quad flat packs (CQFPs), are now being replaced with CGAs with a 1.27- and 1.0-mm pitch (distance between adjacent ball centers) or less [4-16]. CGA packages are preferred to CBGA (see Fig. 1) since they show better thermal cycle solder-joint reliability than their CBGA counterparts. Superior CGA reliability is achieved for larger packages when CBGA resistance to thermal cycling reduced with increasing package size. All ceramic packages with more than about 1000 I/Os come in the CGA style with 1-mm pitch or less to limit growth of the package size.

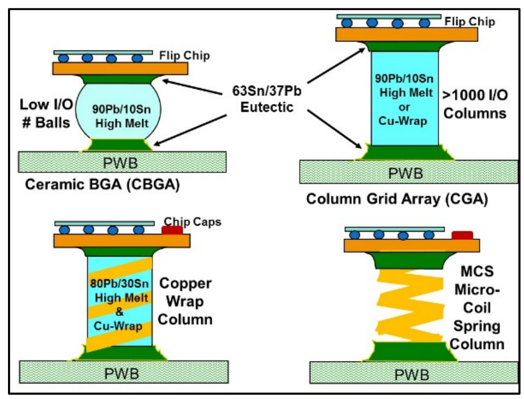

Figure 1. Technology trends from ceramic ball grid array (CBGA) to column grid array (CGA) with solid solder column, copper-wrapped, and micro-coil spring column interconnections.

Key recent trends in CGAs for high reliability applications are as follows:
- CQFPs to area array packages
- CBGAs to CGAs (>500 I/Os) and land grid arrays (LGAs)
- Wire-bond to flip-chip die within a package
- Flip-chip die required underfill and restriction during board level cleaning
- Hermetic to non-hermetic packages (>1000 I/Os), a.k.a class Y
- Addition of high density decoupling capacitors on the CGA ceramic substrate
- High-lead solid solder columns (*PbSn*-column) columns as well as copper wrap (copper-wrapped column (*cw*-column)
- Introduction of beryllium-copper micro-coil spring column (*mcs*-column)

- Pb-Sn to Pb-free, including potential for using a copper column (*cu*-column)
- Land grid with conductive interconnects rather than Pb-free solder

The key drawback of CGAs remains that individual column re-workability is impossible and inspection capability for interconnection integrity is poor (e.g., cannot detect cracks or cold solder). Implementation of process controls for CGA assembly is critical to achieving quality solder joints, which in then provides optimum assembly reliability. Visual inspection of peripheral columns, when they are not blocked, is possible by optical microscopy to assure solder quality as another process indicator. Although progress has been made in improving the resolution of x-ray for better inspection, the issue of inspection for specific defects, such as cold solder joints and microcracks, remains unresolved.

Even though CGAs are commercial-off-the-shelf (COTS) packages, their high reliability versions go through more stringent screening, which adds significant cost and longer delivery times. The issues with CGA COTS packages are essentially the same as other COTS issues and include package die source and lot-to-lot materials variations, availability of packages with radiation-hard die, outgassing for materials including underfill, and so on. A number of these issues are addressed for high reliability versions. Assembly, inspection, and lack of individual solder reworkability issues are additional key aspects of such implementation. Assembly of the high density, high I/Os, and heavy weight of advanced flip-chip CGAs with up to 1752 columns is also challenging and requires additional process optimization.

Synergism of Thermal/Mechanical Loading

In recent years, a number of specifications on thermal cycling and drop and vibration characterization have been generated by commercial industry, particularly by IPC [17] and JEDEC [18]. These specifications add to the wealth of previous specifications by the military, e.g., Mil-Std-810F, updated in 2008 [19], on vibration /shock. Demand for new specifications stem from increasing needs for characterization of advanced electronics that are more susceptible to both thermal and mechanical stresses. The first joint IPC/JEDEC industry specification, IPC 9701, was generated to address specific requirement needed to address the thermal cycle reliability of area array packaging at the 2nd level, assembly.

For mobile electronics, in addition to IPC mechanical bending characterization, IPC/JEDEC 9702 and 9707, IPC 9703 covered generic guidelines for mechanical drop and shock testing. More specifically, JEDEC JESD-B111 was developed for portable electronics in response to the need to define resistance to repeated drops, which is required for mobile applications. The shock pulse requirement to PCB assemblies is defined based on JESD22-B110 condition B with 1500 g, 0.5 millisecond duration, and half-sine pulse. This specification is widely used by industry and data are of valuable for high-reliability applications. JESD-B210A defines resistance to mechanical shock.

In a recent literature review on the response of electronics to mechanical loading [20], Suhir and Ghaffarian reported that dynamic response of materials and structures to shocks and vibrations, including the field of electronics, has always been an important topic of applied science and engineering. In military, avionic, space, automotive, and maritime electronics, dynamic loading occurs during the normal operation of the system, whereas in commercial electronics, dynamic loading takes place during mishandling or transportation of electronic equipment and instrumentation. In addition, random vibrations are often applied as time and cost saving means to detect and weed out infant mortalities, even though a particular product might not be intended for a dynamic environment. The authors' literature survey revealed that the published work on drop testing of electronic equipment is enormous; however, the survey did not include the synergism of thermal and mechanical loading including thermal cycles with vibration or drop. A brief review presented below.

Even though research activities under thermo-mechanical loading, including vibration, are growing, reports on this subject are still limited. One possible reason may be due to difficulty in interpreting the test results of a complex vibration loading. Interpretation becomes even more difficult for synergistic effects of random vibration and inclusion of other environmental exposures, such as isothermal aging and thermal cycling. Wu and Barker [21] divided packaging research in this area into four categories as follows.

1. Those using an empirical model to estimate package life under vibration—the formulas have little or no correlation to the underlying physics or dynamics of the problems
2. Those using analytic models that are based on the physics and dynamics of the problem, but generally involve simplifying the assumptions
3. Those relying primarily on finite element modeling
4. Those relying primarily on experimental approaches, correlating with FEA analysis

Miner's rule has often been used for damage accumulation, but in recent years, the applicability of linear superposition of damage has been questioned for combined sequential or combined thermal cycling and vibration. For example, under concurrent vibration and thermal cycling, Zhao, Basaran, and Cartwright [22] reported their observations from a series of concurrent tests on Sn_{63}/Pb_{37} solder joints for ball grid array (BGA) package and compared them with pure thermal cycling results. They observed that although thermal deformation is the dominant feature of solder-joint behavior, vibration significantly modifies the total behavior of solder joints under concurrent stresses.

For heavy weight power electronics, Dasgupta, Choi, and Habtour [23] also showed that linearized approximations of vibration induced failures can lead to highly misleading and non-conservative predictions of time to failure. They explored the influence of nonlinear dynamic phenomena on damage accumulation under multiaxial vibration excitation. Test results showed that vibration durability decreases as temperature increases above the initial ambient room temperature (25°C). However, no clear trends was observed as temperature decreased. Under multi-axial vibration, the heavy, tall electronic components experience significant nonlinear amplification of stresses and damage.

Another perspective on Miner's rule's inapplicability for damage accumulation was recently presented for the vibration of area array package assembled with lead-free solder [24]. Fatigue life under vibration is usually limited by crack propagation in solder joints if the packaging system is not weakened by pad cratering or intermetallic failures. The authors attributed the inapplicability of Miner's rule to differences in creep mechanisms for thermal cycling and vibration. This indicates that the dominant creep mechanism in vibration may be "diffusion controlled", rather than the dislocation climb controlled mechanism. The different mechanisms may explain the inaccuracy in projection, often by orders of magnitude, when linear superposition is used to account for the effects of vibration cycling amplitude (frequency) variations on life.

Kim and Hwang [25] experimentally investigated the robustness of PBGAs for space application by subjecting a number of assemblies to vibration under 22.48 g_{rms} level for one minute and under 31.78 g_{rms} for two minutes. The vibration was followed by sixteen thermal cycles in the range of –30°C to 65°C, each with two hour dwell. At these levels of vibration, the assemblies with or without underfill did not show any solder joint failures. When vibration time extended; however, assemblies without underfill showed solder-joint failures at the edge of the chip. The authors recommend using underfill for PBGAs with larger dies because they are more susceptible to vibration failures.

M. Cole et al. [26] presented cycles-to-failures after vibration for both CBGA and CGA assemblies. Mil-STD 810E was used to generate impact and vibration data for their test vehicle. There were no failures of CBGAs or CGAs after vibration with heatsink of 73 g. However, CGAs with heatsink weights of 100 and 150 grams failed, but CBGAs showed no failures under these weights. Cracks were induced in CBGAs in the eutectic tin–lead solder either in package or board sites when subjected to 7.73 g_{rms} in 20-2000Hz frequency ranges.

It was reported that for CBGAs, crack initiations were similar to those of accelerated thermal cycling (ATC), but with no deformation (grain growth) typically present in ATC. Also, thermal mismatch induces both shear and tensile, but vibration induces primarily tensile and did not cause local deformation. For CBGA with heat sink lower than 150 grams, there were no synergistic effects of initial shock/vibration. Also, no statistical differences were found between those with initial shock and vibration and those without a priori test.

For CGA with solid solder ($Pb_{90}Sn_{10}$) columns, Perkins and Sitaraman [27] developed a nonlinear damage model to account for non-linearity of thermal cycle and vibration. It was shown that the TC+Vib sequence (thermal cycling followed by vibration loading) was a harsher sequence than the Vib+TC sequence (vibration loading followed by thermal cycling). The difference was attributed to the severe deformation and microstructural changes that occur in thermal cycling, which initiate cracks quickly and accelerates the subsequent vibration loading. A universal equation was developed for thermal cycle behavior of CBGA and CGA using design of simulation (DOS) by finite element modeling. The equations show that the effect of DNP (package size) becomes negligible for a constant CGA pitch.

Authors referring to an earlier work by Ghaffarian state that the actual test results contradicted the FEA projection. Test results show that for the same pitch CBGA/CGA, larger DNP reduces the fatigue life of the outermost solder balls/solder columns. After justification for a potential process difficulty of a larger part, Perkins concluded that "this indicates a weakness in the FEM regarding the substrate size effect only." The author suggested that further modeling work, along with experimental tests where substrate size is the only variable to change, are necessary to determine a better correlation.

Tripathi, et al. [28] performed thermal cycle (100 cycles, –55/105°C) testing on the CGA1144 (solid solder column) assemblies for space applications. The thermal cycle was followed by sine, random vibration (normal/in plane, 17.5/11.8 g_{rms}, 2 min) PCB, and shock (normal/in plane 700/400 g, 5 shock). These tests simulate the launch, booster separation, and in-orbit vibrational loads representing a spacecraft's environmental conditions. No degradation was detected to the solder joints after 100 thermal cycles followed by mechanical testing. The favorable results indicate the robustness of CGA1144 assemblies and fixture design. There were no signs of necking or bending of the columns after 100 thermal cycles. However, after 1200 thermal cycles, shifts in columns and cracking in solder joints were observed, but there were no failures.

Ying, D, et al. [29], presented the effect of a priori vibration on subsequent thermal cycling. The CGA package used for evaluation was relatively small (25x25 and 5 mm thick), 1.27 mm pitch, with 349 large solid solder columns (Pb_{90}/Sn_{10}) and it was attached with eutectic tin–lead solder onto PCB. It was subjected to sinusoidal vibration in the z axis (12-18 g) and random vibration of 20.8 g_{rms} with 2 minute duration. The random vibration in the x and y directions was 16.6 g_{rms}. Thermal cycle in the range of –55°/100°C induced severe microcracking up to 90%

coverage at the periphery columns whereas the center columns did not show microcracking. However, no microcrackings were observed under the same condition when the PCB was stiffened by divider rims which engulfed the CGA assembly were added.

Jennings [30] investigated the impact of aerospace high-level g vibration for CGA624 (1.27 mm pitch) and CGA1272 (1 mm pitch) with copper-wrapped columns. Test results presented for vibration alone and in sequential combination with temperature cycling (–40°/100°C). The vibration g-level was 29.8 g_{rms} (average power spectral density (PSD) = 0.084 g^2/Hz) for airborne and 44.7 g_{rms} (PSD = 0.2 g^2/Hz) for space application. When vibration is sequenced with thermal cycling, the level of vibration reduces to 0.066 and 0.099 g^2/Hz with time duration of 1 hour and 3 minutes, respectively.

The two CGA assemblies showed closely similar failure cycles and rates under airborne or space level vibration, possibly due to similarity of "mass per interconnection being about 0.02 grams" for both. The lifespan for both CGAs decreased more than 10x for a 14.9 g_{rms} increase in vibration level. Sequential vibration and thermal cycling showed an early failure for CGA624 and reduced life span for CGA1272 with low-level g, but longer time duration (1 hour).

Multiple failure mechanisms are active in combined environmental testing. The vibration only failures match those of standard fatigue behavior of high lead solder, but cracks in solder column diverted around the copper-wrap of column. Behavior under thermal cycle only or vibration and thermal cycle appeared as expected — stress relaxation, recrystallization, and grain growth showing rough and graininess appearance were observed.

CGA1272 TEST VEHICLE DESIGN, BUILD, AND INSPECTION

To determine assembly reliability of the CGAs with daisy-chain packages, including CGA1272, the board was designed to match CGA patterns. Not all package styles from a manufacturer come in daisy-chain form; generally, manufacturers only select representative packages and offer them as a daisy chain, so the choice of packages for evaluation are limited. The daisy chain patterns on PCB were designed to complement CGA patterns, forming a complete loop after assembly. The resistive loop is generally monitored during thermal cycling to allow detection of open loops due to solder-joint opens of CGAs onto PCB. The two daisy chain CGA packages, even though built by two different manufacturers, had roughly the same column dimensions.

A complex PCB was designed to accommodate the CGA packages and provide sites for other advanced fine-pitch array and leaded/no-lead packages. Figure 2 shows the board design, with a daisy chain pattern, and how traces are routed to the edge of the board for daisy chain monitoring.

A design of experiments (DOE) technique was used to cover various aspects of processing and packaging assembly reliability. The following packages and parameters were evaluated as part of a larger DOE implementation:

- The CGA1272, with 1.0-mm pitch and 37.5-mm^2 body size, designed with enough space for rework evaluation. Lead parts are designed to determine the influence of rework visually. Numerous daisy chains were designed on board to complement daisy chains on a package, in order to generate complete chains for solder-joint failure monitoring. Probe pairs were added near packages to monitor subdivided daisy chains.

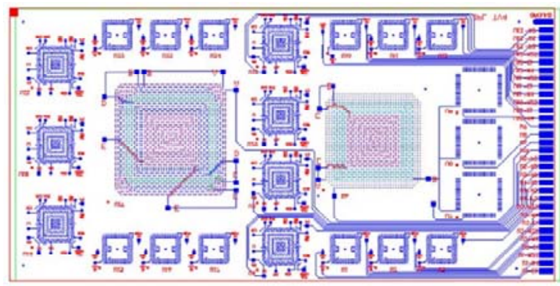

Figure 2. Test vehicle design showing CGA1272 (center right) daisy chain patterns.

- Boards were made from high glass transition temperature (Tg) FR-4 materials with 0.093-inch thickness. They had a hot air solder leveling (HASL) tin–lead surface finish commonly used for tin–lead solder.
- A standard 6-mil-thick stencil was used for paste printing of the whole board when only the two CGAs are to be built. However, other stencil thicknesses or use of a mini stencil may be required to accommodate building a board of this complexity, or if reworking is performed.
- Three types of solder paste were evaluated for paste print quality. Solder paste volumes were measured at the four corners and at the center of several assemblies to document actual paste print volume, distribution, and solder paste release efficiency.
- Vapor phase reflow was used to assemble the two CGA packages. Placement of CGAs, however, was done using a rework station.

These assemblies (see Figure 3) were first subjected to inspection and daisy-chain continuity checks to determine manufacturing robustness of various package configurations. They were then exposed to a number of environmental conditions to evaluate their reliability and failure mechanisms. Both the paste print quality evaluation and inspection observation after assemblies are discussed below.

Figure 3. An assemble test vehicle design showing CGA1272 (right) and CGA 1752 (left).

X-ray inspection was performed, following visual inspection and the daisy-chain continuity check, to selectively verify package/assembly conditions. The 2D real time x-ray transmission system with oblique angle views was utilized for this inspection. Figure 4 shows representative x-ray photomicrographs for the CGA1752 and CGA1272 packages after assembly.

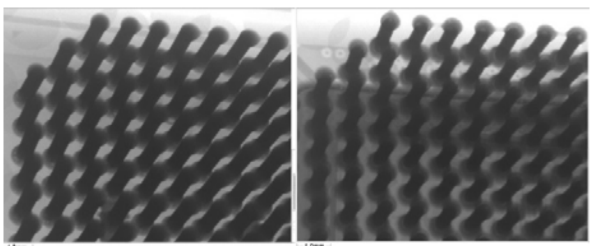

Figure 4. As-assembled X-ray photomicrographs for the CGA1272 (right) and CGA1752 (left). There were no signs of shorts.

Visual inspection of peripheral columns was also performed for most assemblies, since the board was designed for visual characterization (most of the PCBs were only populated with CGAs). Only outer rows, and in some cases, second and third rows could be assessed for solder-joint quality. The representative photomicrographs in Fig. 5 show the quality of solder joints for CGA1752 and CGA1272 assemblies. Note that solder-joint fillet formations are different for the pure-solder column and copper-wrapped solder columns. Solder joints were generally acceptable even though they appear to have different wetting angles and column peripheral coverages.

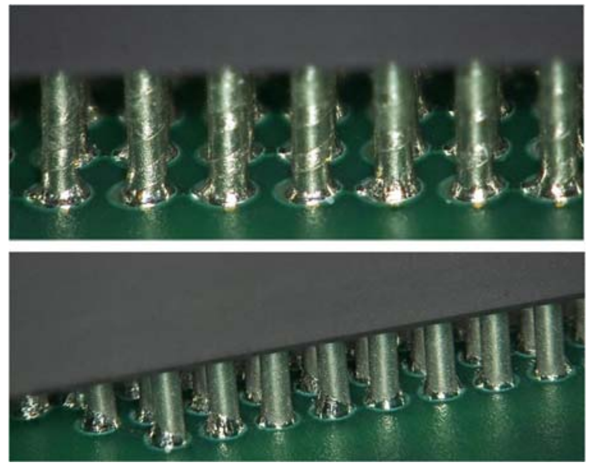

Figure 5. Representative photomicrographs of solder-joint quality after assembly for CGA1272 (top) and CGA1752 (bottom).

CGA1272: Damage Progression with Thermal Cycling (–55°/100°C)

The CGA1272 and CGA 1752 assemblies were subject to thermal cycling in the range of –55 to 100°C with a 2 to 5°C/min (3°C/min) heating/cooling rate. Dwells at extreme temperatures were about 15 minutes with duration of 140 minutes. Damage progression with thermal cycling was established using an optical microscope. Figure 6 presents representative photomicrographs of solder-joint condition and damage progression due to thermal cycling for CGA 1272 in the range of –55° to 100°C up to 200 cycles.

CGA1272 with copper-wrapped column showed good solder-joint uniformity and wetting, and concave solder surrounding columns. Minimal solder damage was detected due to 100 thermal cycles that slightly increased at 200 cycles; solder/columns showed signs of graininess representing tin–lead solder grain growth due to exposure at 100°C during thermal cycling. Column distortions were minimal, except for graininess of solder exposed between the copper wrap at 200 thermal cycles. In addition, there were minimal apparent column shifts due to shear-induced deformation resulting from CGA/PCB CTE mismatches during thermal cycling.

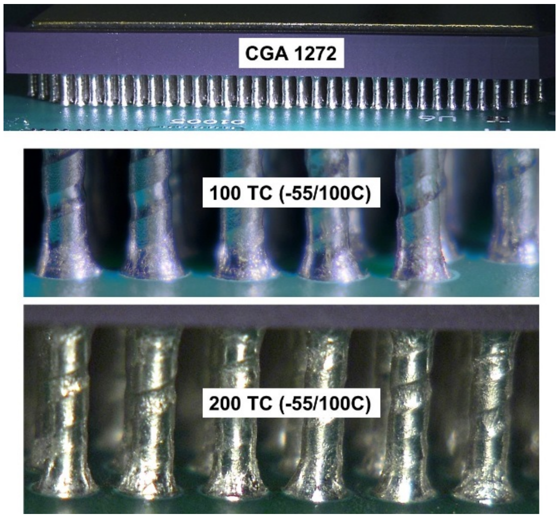

Figure 6. Representative photomicrographs of solder-joint quality after 100 and 200 thermal cycles (–55/100°C) for CGA1272 assemblies.

CGA1272 Damage Progression with Thermal Cycles (–55°/125°C)

The CGA 1272 assemblies were also subjected to a more extreme cycle in the range of –55 to 125°C with a 2° to 5°C/min (3°C/min) heating/cooling rate. Dwells at extreme temperatures were about 15 minutes with duration of 210 minutes for each cycle. Visual inspection was performed to establish damage progression of outer columns of CGAs at thermal cycling intervals by optical microscopy. Figure 7 presents representative photomicrographs of solder-joint condition and damage progression due to thermal cycling in the range of –55 to 125°C at 200 cycles. Figure 8 show results at 500 cycles. Damage due to thermal cycling, noticeable from these photomicrographs, can be categorized as follows:

CGA1272 with Cu spiral column showed good solder-joint uniformity and wetting. Some solder damage at 200 cycles showed signs of graininess representing of tin–lead solder grain growth due to exposure at 125°C during thermal cycling. Column distortions were minimal, except for signs of graininess of solder between copper wrap, at 200 thermal cycles with no apparent column shifts due to thermal cycling. Damage indicated by graininess solder slightly increased at 500 thermal cycles.

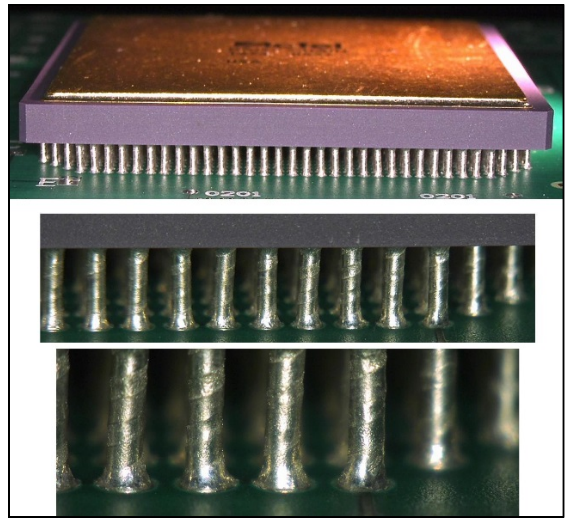

Figure 7. Representative photomicrographs of solder-joint quality after 200 thermal cycles (–55/125°C) for CGA1272.

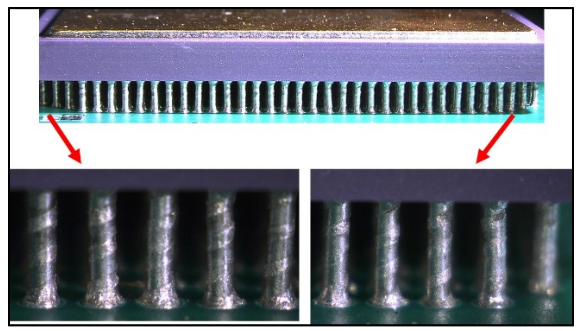

Figure 8. Representative photomicrographs of solder-joint quality after 500 thermal cycles (–55/125°C) for CGA1272.

Drop before thermal cycle

The test vehicles with CGA1272 (copper-wrapped column), as assembled and after thermal cycling, were subjected to drop testing to determine synergistic effects of thermal cycle first and then shock/drop condition. Figure 9 shows drop test set up (top), a daisy-chain pattern (bottom right), and a table listing the number of drops from a 36-inch height. Daisy-chain resistances were recorded at room temperature after each drop. The number of drops from the 36-inch height for an "as assembled" CGA1272 (SN03) with a no priori thermal cycle condition is also tabulated.

This assembly failed from the center rows of columns (C-C daisy-chain pattern) after the first drop, then, it failed from the outer rows of columns (A-A) after fifteen (15) drops, but with no failure of the middle columns (B-B) to 16 drops before removal for optical microscopy and SEM failure analyses. The occurrence of the first daisy-chain failure from the center of C-C daisy-chain pattern was unexpected since it was thought that the outer row of columns (C-C) should have failed first considering the highest deflections occur at the package periphery, especially at the corner solder columns. It is unknown if workmanship had played a role in such an early inner daisy-chain failure. The first failure occurrence of the "as assembled" CGA rather than the ones with an initial thermal cycle will be discussed later based on the potential dominant failure mechanisms.

# of Drops (36 In)	S/N 35 As Assembled		
	A-A Outer	B-B Middle	C-C Inner
1	1.81	2.65	open
2	1.81	2.67	open
3	1.80	2.86	open
4	1.79	2.88	open
5	1.79	2.89	open
6	1.80	2.90	open
7	1.80	2.94	open
8	1.80	2.94	open
9	1.79	2.94	open
10	1.80	2.95	open
11	1.80	2.96	open
12	1.80	2.96	open
13	1.81	2.99	open
14	1.79	2.99	open
15	open	2.99	open
16	open	3.04	open
	Remove for Optical/SEM		

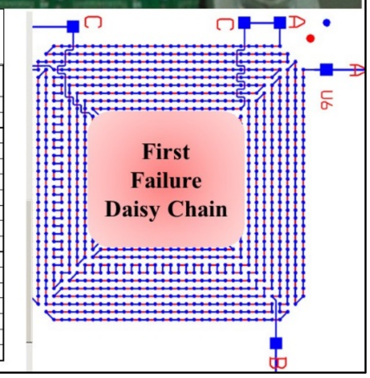

Figure 9. Drop test set up (top), daisy-chain patterns (bottom right), and number of drops to failures for CGA 1272 I/O assembly.

Figure 10 shows optical and SEM representative photomicrographs of CGA1272 after sixteen drops. At least three types of failures were apparent: column failures, PCB pad separation, and daisy chain trace failures. The optical/SEM photomicrographs of two columns side-by-side clearly show two failure types: (1) failure within column, it is severely cracked and even dislodged with pieces of solder extruding from the copper-wrapped section, and (2) failure from a separation of the pad from the PCB in a neighboring column.

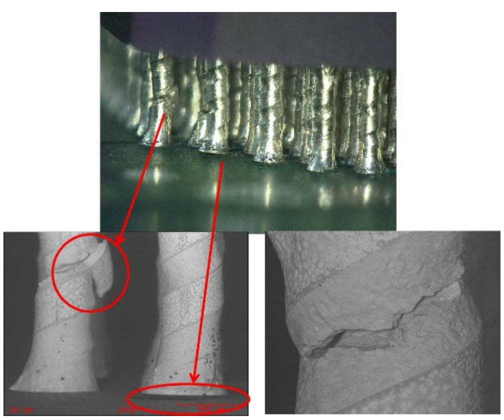

Figure 10. Optical photomicrographs and SEM of SN35, as assembled CGA1272, failed after first drop, but removed after 16 drops show three key failure mechanisms, column failure, pad separation, and trace failure.

Different failure mechanisms indicate the weak link of interconnection elements (i.e., package pad, column, PCB pad) since proximity of columns indicates the proximity of loading. After further inspection, it becomes apparent that failure for this column occurred at the board site, a smooth separation gap between column and pad bonding, which generally is known as pad cratering when separation distorted by multiple cracks and rough surfaces. Is this a pad cratering or copper-pad separation is yet to be determined.

Lall et al. [31] reported that column failures were the dominant failure mechanism for CGA400 with micro-coil spring and solid solder columns when subject to a typical 1500 g and very-high g levels of up to 50,000 g. MCS failed in the spring and solid-solder columns showed failures in the column after ductile necking and failure [32]. CGAs with 400 MCS (array 20x20) had similar configurations and build by MSFC as reported for those of CGA 1517 I/O, they were attached to the package with SAC305. Both CGAs were assembled onto the PCBs with eutectic tin–lead solder. The number of drops to failure for both CGAs at 30,000, 40,000, and 50,000 g-levels were established and plotted in graphs. It was shown that the number of drops to failure decreases with the increase in g-level from 30,000g to 50,000g. The micro-coil spring outperformed the solid solder column interconnect at these high g-levels.

Drop after Thermal Cycles

A number of CGA1272 assemblies, each with a priori thermal cycles, also were subjected to drop testing. Table 3 shows the serial number of assemblies with the number of initial thermal cycles and temperature ranges. The SN01, SN02, and SN12 were subjected to thermal cycle in the range of –55°/125°C for 300, 400, and 500 cycles, respectively. SN04 is the only assembly that was subjected to –55°/100°C for 500 cycles. Contrary to the first drop failure of as assembled SN035, all thermally cycled CGA1272 assemblies did not show signs of failure up to 30 drops from a 36-inch height.

Table 3. Number of drops at 36 and 48 inch height for CGA1272 with different initial thermal cycles.

Number of Drops (36 Inches Height)	S/N 01 300 Thermal Cycles (-55°/125°C)			S/N 02 400 Thermal Cycles (-55°/125°C)			S/N 04 500 Thermal Cycles (-55°/100°C)			S/N 12 500 Thermal Cycles (-55°/125°C)			S/N 35 As Assembled		
	A-A	B-B	C-C	A-A	B-B	C-C	A-A	B-B	C-C	A-A	B-B	C-C	A-A	B-B	C-C
1	1.94	2.54	2.15	1.87	2.46	2.06	1.91	2.51	2.11	1.90	2.52	2.12	1.81	2.65	open
14	1.90	2.51	2.13	1.86	2.44	2.05	1.90	2.49	2.09	1.87	2.48	2.10	1.79	2.99	open
15	1.91	2.53	2.14	1.87	2.46	2.05	1.91	2.49	2.10	1.88	2.49	2.10	open	2.99	open
16	1.90	2.52	2.14	1.91	2.46	2.04	1.93	2.50	2.11	1.88	2.48	2.10	open	3.04	open
17	1.91	2.51	2.14	1.87	2.45	2.05	1.91	2.52	2.13	1.91	2.51	2.18	STOP	STOP	STO
18	1.92	2.53	2.13	1.86	2.50	2.05	1.92	2.50	2.11	1.88	2.49	2.18	Removed for Failure Analysis		
19	1.92	2.53	2.15	1.88	2.51	2.06	1.92	2.51	2.10	1.93	2.50	2.11			
20	1.95	2.60	2.15	1.87	2.47	2.06	1.92	2.51	2.11	1.94	2.54	2.14			
Drop (48 Inches)	S/N 01			S/N 02			S/N 04			S/N 12					
	A-A	B-B	C-C	A-A	B-B	C-C	A-A	B-B	C-C	A-A	B-B	C-C			
1	1.93	2.54	2.14	1.88	2.46	2.06	1.93	2.51	2.12	1.90	2.50	2.13			
28	1.93	2.52	2.14	1.88	2.46	2.06	1.91	2.51	2.11	1.90	2.50	2.14			
29	3.98	2.53	2.14	1.87	2.45	2.05	1.91	2.50	2.12	1.87	2.50	2.12			
30	open	2.53	2.15	1.89	2.47	2.07	1.93	2.51	2.13	1.90	2.52	2.11			
31	open	2.53	2.15	1.89	2.47	2.09	1.92	2.51	2.12	1.91	2.52	2.13			

Figure 11 shows the acceleration g level for the 36 inch drop level. It reaches to about 908 g and then is rapidly attenuated. Because of no failure in 20 drops, it was decided to accelerate failure by increasing the height of the drop to the maximum available level of this specific equipment. A number of adjustments, including adding additional cushion, need to be done in order to minimize bouncing back upon the drop.

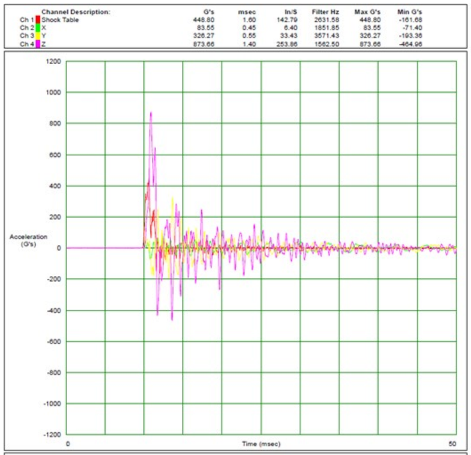

Figure 11. Acceleration in g level versus time for the drop of CGA1272 assemblies at 36-inch height

The CGA1272 with 300 initial thermal cycles (–55°/125°C) showed the first failure after addition of 29 drops at 48-inch height (20 drops at 36 inches plus 29 drops at 48 inches). The failure occurred at the outer rows of daisy-chain pattern. There were no failures of the other assemblies up to 31 additional drops at 48-inch height. It is interesting to note that the SN01 failed had the lowest number of cycles (300 cycles) compared to the other two assemblies (with 400 and 500 thermal cycles). However; the SN01 was subjected to an additional one hour vibration as discussed in reference [4]. The results contradict the notion on the synergistic effects of thermal cycle, vibration, and drop testing. The potential cause of such contradiction is presented in the discussion section.

Figure 12 shows optical photomicrographs of the failed SN01 CGA1272 assembly after red dye exposure prior to pull testing in preparation to determine failure mechanisms. It clearly shows several solid solder column failure with the copper wrap still intact. As stated earlier, the SN01 was subjected to 300 thermal cycles in the range of -–55° to 125°C and one hour of vibration at about 9 grms. It showed no failure after vibration. It was subjected to drop testing which again showed no failure at 20 drops from 36 inches. However, the outer daisy chain failed after an additional 30 drops from 48 inches.

Figure 12. Optical photomicrographs of SN01, CGA1272 assembly after 300 cycles + 1 hour vibration, which showed no failure at 20 drops from 36 inches, the outer daisy chain failed after an additional 30 drops from 48 inches, showing red dye in preparation (top) and after pull without complete separation.

Thermal Cycle after "TCs+ Drops"

The test results of test vehicle with prior thermal cycles and failure or no failure after two drop conditions are summarized in the following.

SN035, as assembled, internal daisy chain failed after the first drop from 36-inch height. The testing was continued until the outer-row daisy chain failed after 15 drops.

SN01, 300 TC (–55°/125°C), showed no failure at 20 drops from 36 inches. The outer daisy chain failed after an additional 30 drops from 48 inches. This assembly was subjected to one hour of vibration after thermal cycling with no failures.

SN02, 400 TC (–55°/125°C), showed no failure at 20 drops from 36 inches, also showed no failure after additional 31 drops from 48 inches.

SN04, 500 TC (–55°/125°C), showed no failure to 20 drops from 36 inches, and also showed no failure after an additional 31 drops from 48 inches.

SN12, 500 TC (–55/100C), showed no failure at 20 drops from 36 inches, and also showed no failure after an additional 31 drops from 48 inches.

Figure 13 shows representative X-ray photomicrographs for SN35 and SN01 with failure after a number of drops and SN04 with no failures after drops. The SN04 and the SN12 CGA1272 assemblies, which showed no failure after drops, were subjected to a number of additional thermal cycles to determine if there were early failures that were possibly not detected by drop testing which could be possibly detected by thermal cycling.

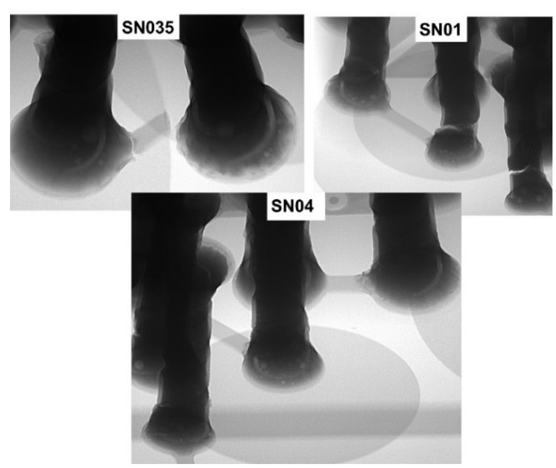

Figure 13. Representative of X-rays for SN35 and SN01 with failure after drop and TCs+drops, and SN04 with no failure after TCs+drops..

Figure 14 shows representative optical photomicrographs of column and solder joints for the SN04 CGA1272 assembly after 200 thermal cycles in the range of (–55°/125°C). Note this assembly prior to drop testing had 500 cycles (–55°/100°C). No failure condition was verified by visual inspection and daisy-chain continuity checking.

Figure 14. Optical photomicrographs of the SN04, CGA1272 assembly after 500 cycles (–55°/100°C), with no failure at 20/30 drops from 36/48 inches and 200 additional thermal cycles (–55°/125°C).

Figure 15 shows representative optical photomicrographs of columns and solder joints for SN12 after 100 additional thermal cycles (–55°/125°C). Note this assembly had 500 thermal cycles of –55° to 125°C, prior to drop testing. No failure was observed either by visual inspection or daisy-chain verification. No further thermal cycling was performed to determine failure after TCs+Drops+TCs.

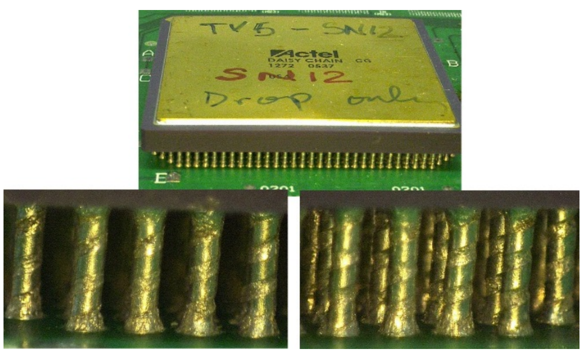

Figure 15. Optical photomicrographs of the SN12, CGA1272 assembly after 500 cycles (–55°/125°C), with no failure at 20/30 drops from 36/48 inches and 100 additional thermal cycles (–55°/125°C).

TC Projection BGA/CGA

Suhir, et al. [33-36] developed analytical equations for BGA/CGA assemblies under thermal stresses using various solid mechanics methods. A tri-materials stress-analysis method was used to analytically compare the effect of a double-sided assembly with a mirror-image configuration. The model assumes the use of a short cylinder (beam) that is subjected to bending representative of columns in CGA. The beam's ends are considered to be clamped and offset. The offset in CGA (Δ) is estimated from the thermal-mismatch strain between the CGA and the PCB for a given joint as function of its DNP. The analyses are limited to elastic deformation only.

The following formulas were derived for the maximum shear and normal stresses by assuming a short cylinder (beam) of diameter d and height h (length). The beam's flat ends are clamped and offset at the given distance of Δ.

$$\tau_{\max} = \frac{9}{8} E \frac{\Delta}{d}\left(\frac{d}{h}\right)^3 \left[1 + \frac{27}{10}(1+\nu)\left(\frac{d}{h}\right)^2\right], \qquad (2)$$

$$\sigma_{\max} = 3E\frac{\Delta}{d}\left(\frac{d}{h}\right)^2\left[1 + \frac{27}{10}(1+\nu)\left(\frac{d}{h}\right)^2\right] = \frac{8}{3}\frac{h}{d}\tau_{\max}. \qquad (3)$$

Here ν is Poisson's ratio of the material.

These equations indicate that for a beam analysis, the normal bending stress always exceeds the shearing stress (8/3 (h/d) >1 since h>d). For the height/diameter (h/d) ratio of above 12-15, these relationships confirm the well-known condition that the shear stress does not have to be accounted for. This statement is true whether one uses the classical Timoshenko model— the displacement of a cantilever beam subjected to a force applied to the beam's end— or uses this analysis when the maximum force and the corresponding stresses are given as an end's offset.

The stress analyses were expanded to determine thermally induced stresses in BGA and CGA assemblies using three steps. As an example, the calculation for the maximum interfacial shear stresses for BGA/CGA are shown in the following.

$$\tau_{\max} = k_* \frac{\Delta\alpha\Delta t}{\lambda_*} = 0.8294x\frac{0.0017}{72.3701x10^{-5}} = 1.9483 kg/mm^2$$

(BGA)

$$\tau_{\max} = k_* \frac{\Delta\alpha\Delta t}{\lambda_*} = 0.6278x\frac{0.0017}{72.3701x10^{-5}} = 1.4747 kg/mm^2$$

(CGA)

Thus, the use of CGA resulted in about 24 percent relief in the maximum interfacial shearing stress. The corresponding angular (shearing) strains for BGA and CGA are as follows:

$$\gamma_{\max} = \frac{\tau_{\max}}{G} = \frac{1.9483}{2040.7} = 9.5472x10^{-4} = 0.09547\%$$

(BGA)

$$\gamma_{\max} = \frac{\tau_{\max}}{G} = \frac{1.4747}{2040.7} = 7.2264x10^{-4} = 0.07264\%$$

(CGA)

Drop Projection for BGA/CGA

Suhir and Ghaffarian [37] developed a new methodology to determine the stresses due to drop for BGA/CGA and if CGA flexibility also plays key role in robustness of CGA under dynamic loading. It is thought that even though the application of the CGA technology to relieve thermal stresses in the solder material is effective, it might be less effective when the PCB/package experiences dynamic loading. The ineffectiveness might be due to the weight/mass of the CGA on solder joints being larger than BGA out weighing the CGA column flexibility. The numerical example carried out for an arbitrary condition: CGA has about four times weight distribution/thickness than its BGA counterparts.

Discussion

The analytical results indicate that drop-impact induced stresses in solder joints can significantly exceed the thermal stresses — maximum shear stresses (Kg/mm^2) of 14.33 and 15.28 for BGA and CGA, respectively. The maxim peeling stresses had similar trends, but higher values, showing 22.73 and 23.98 (Kg/mm^2) for BGA and CGA, respectively.

The question is why the thermal cycle preconditioning helped to improve resistance to drop-test impacts. Understanding the competing failure mechanisms may help to interpret the test results. The key contributors to failure mechanisms are:

1. PCB pad failure by the pad cratering and separation/dis-bonding
2. PCB trace failure by separating the daisy chain trace patterns
3. Failure at the intermetallic interface
4. Failure in solder joints either at the PCB- or package-sites
5. Failure at the columns, either Cu-wrap or solder column section

Previously, it was shown that the column did not degrade significantly with thermal cycling. Solder joints in assembly, however, are significantly degraded with thermal cycles. If it is assumed that the pad cratering is the predominant failure mechanism, then, a weakened solder by thermal cycling (grain growth and microcracked condition) transfers a lower load to the pad interface. Thus, a lower potential for pad cratering. To shed further light on these failure mechanisms, more systematic testing should be performed.

SUMMARY

Within the last decade, the use of CGA for high reliability applications has shown significant growth; however, test data is scarce, especially for newer CGA with larger than thousand I/Os. Reliability test data were presented for CGA1272 with copper-wrapped columns under accelerated thermal cycling conditions along with their failure mechanisms.

Test results are also presented for failures of CGA1272 under sequential thermal cycles, drops, and thermal cycles. Simple analytical models were developed to project stresses/strains for BGA/CGA under thermal cycling and drop testing. Our test data, as well as data presented in literature for CGAs or BGAs, does not show a clear trend as a dominant damaging mechanisms for a synergism effects of sequential or combined environmental exposures. CGA1272, unexpectedly, "as assembled" package, failed before those with initial thermal cycle exposures. One possible reason for this earlier failure is pad cratering, and stiffer solder joints for "as assembled" test vehicle. More work on these topics should shed light on answering many questions on understanding failure mechanisms under single, as well as sequential or combined thermos-mechanical, testing.

ACKNOWLEDGEMENTS

The research described in this publication is being conducted at the Jet Propulsion Laboratory, California Institute of Technology, under a contract with the National Aeronautics and Space Administration. © 2016 California Institute of Technology. Government sponsorship acknowledged.

The author would like to acknowledge team members at JPL, Professor S.M. Ramkumar and students at Rochester Institute of Technology, and Dr. E. Suhir at ERS for their support in assembly, thermal cycling, failure analysis, drop tests, and developing analytical models. The author extends his appreciation to program managers of the National Aeronautics and Space Administration Electronics Parts and Packaging (NEPP) Program.

REFERENCES

[1] Ghaffarian R. Update on CGA packages for space applications. *Microelectronics Reliability*. 2016 Jan 15.

[2] Ghaffarian, R. "CCGA Packages for Space Applications," *Microelectronics Reliability*, vol. 46, pp. 2006–2024, 2006.

[1] *International Technology Roadmap for Semiconductors*, ITRS (website), http://www.itrs.net/, accessed Nov 15, 2015.

[2] International Electronics Manufacturing Initiatives (website), INEMI, http://www.inemi.org/, accessed Nov. 15, 2015.

[3] IPC, Association Connecting Electronics Industry (website), http://www.ipc.org, accessed Nov. 15, 2015.

[4] Ghaffarian R. Update on CGA packages for space applications. *Microelectronics Reliability*. 2016 Jan 15.

[5] Ghaffarian, R. "CCGA Packages for Space Applications," *Microelectronics Reliability*, vol. 46, pp. 2006–2024, 2006.

[6] Ghaffarian, R., Evans, J.W., "Enabling More than Moore: Accelerated Reliability," (website) https://sma.nasa.gov/docs/default-source/News-Documents/newsfeed-astr-paper.pdf?sfvrsn=2

[7] Ghaffarian, R., "Defect Features Detected by Acoustic Emission for Flip-Chip CGA/FCBGA/PBGA/FPBGA Packages and Assemblies," IPC/APEX Conference Proceedings, Las Vegas, NV, March 16-17, 2016

[8] Ghaffarian, R., "Effect of Column Properties and CGA Assembly Reliability by Testing and Analysis," in

Proceedings of IEEE InterSociety Thermal Conference (iTherm) , Las Vegas, NV, May 31st –June 3rd , 2016
[9] Ghaffarian, R. "Damage and Failures of CGA/BGA Assemblies under Thermal Cycling and Dynamic Loadings," *ASME 2013 International Mechanical Engineering Congress and Engineering. IMECE2013*, November 15-21, San Diego, California.
[10] Ghaffarian, R., "Reliability of Column/Board CCGA Attachment," *IEEE InterSociety Thermal Conference (ITherm)*, San Diego, CA May 31–June 2, 2012.
[11] Ghaffarian, R., "Assembly and Reliability of 1704 I/O FCBGA and FPBGA," in *Proceedings of IPC/APEX*, San Diego, CA, Feb.28–March 1, 2012.
[12] Ghaffarian, R., "Thermal Cycle and Vibration/Drop Reliability of Area Array Package Assemblies," Chapter 22 in *Structural Dynamics of Electronics and Photonic Systems*, eds. E. Suhir, E. Connally, and D. Steinberg Springer, 2011.
[13] Ghaffarian, R., "Thermal Cycle Reliability and Failure Mechanisms of CCGA and PBGA Assemblies with and without Corner Staking," *IEEE Transactions on Components and Packaging Technologies*, vol. 31, issue 2, June 2008.
[14] Tasooji, A., Ghaffarian, R., and Rinaldi, A. "Design Parameters Influencing Reliability of CCGA Assembly and Sensitivity Analysis," *Proceedings of ITherm*, San Diego, CA (May 30-June 2, 2006.
[15] Ghaffarian, R., "Area Array Technology for High Reliability Applications," Chapter 16 in *Micro-and Opto-Electronic Materials and Structures: Physics, Mechanics, Design, Reliability, Packaging*, ed. E. Suhir, Springer, 2006.
I16] Ghaffarian, R., "BGA Assembly Reliability," Chapter 20 in *Area Array Packaging Handbook*, ed. K. Gilleo, McGraw-Hill, 2002.
[17] IPC, Association Connecting Electronics Industry, http://www.ipc.org/Default.aspx, http://www.ipc.org/4.0_Knowledge/4.1_Standards/SpecTree.pdf., accessed June 29, 2013
[18] JEDEC, http://www.jedec.org/, accessed Nov. 15, 2015.
[19] DLA Land and Maritime, http://www.landandmaritime.dla.mil/Programs/MilSpec/DocSearch.aspx., accessed Nov. 15, 2015.
[20] Suhir, E., Ghaffarian, R., "Predictive Modeling of the Dynamic Response of Electronic Systems to Impact Loading: Review", submitted to ZAMM (Zeitschrift fur Angewandte Mathematik und Mechaniksubmitted), 2016
[21] Wu, M.L., Barker, D., "Rapid Assessment of BGA Fatigue Life under Vibration," *IEEE Transactions on Advanced Packaging*, 2009.
[22] Zhao, Y., Basaran, C., and Cartwright, A., "Inelastic Behavior of Microelectronics Solder Joints under Concurrent Vibration and Thermal Cycling," *Thermal and Thermomechanical Phenomena in Electronic Systems, 2000. ITHERM 2000*. The Seventh Intersociety Conference on, vol.2, no., pp.174–180 vol. 2, 2000.
[23] Dasgupta, A, Cholmin, C., and Habtour, E.,. "Keynote: Simulation and Test Vibration-Nonlinear Dynamic Effects in Vibration Durability of Electronic Systems." In *Integrated Power Systems (CIPS), 2014 8th International Conference on*, pp. 1-10. VDE, 2014.
[24] Batieha, F., S. Hamasha, Y. Jaradat, L. Wentlent, A. Qasaimeh, and P. Borgesen. "Challenges for the prediction of solder joint life in long term vibration." In *Electronic Components and Technology Conference (ECTC), 2015 IEEE 65th*, pp. 1553-1559. IEEE, 2015.
[25] Kim, Y. K., Hwang, D.S., "PBGA Packaging Reliability Assessments under Random Vibrations For Space Applications," *Microelectronics Reliability* 55, no. 1 (2015): 172-179.
[26] Cole, M., Kastberg, E., and Matin, G., "Shock and Vibration Limits for CBGA and CCGA", *Surface Mount International Proceedings*, 1996, pp.89-94
[27] Perkins, A., Sitaraman, S.K., "A Study into the Sequencing of Thermal Cycling and Vibration Tests," *Electronic Components and Technology Conference*, ECTC 2008. 58th, vol., no., pp.584-592, 27–30, May 2008.
[28] Tripathi, S., Hitesh M. P., Shrikant P., Deep K.P., Ishwar, L.P., Chandresh N.J., Rakesh S.S., and Rajkumar, A., "Ceramic Column Grid Array Assembly Qualification and Reliability Analysis for Space Missions." *Components, Packaging and Manufacturing Technology, IEEE Transactions on* 5, no. 2 (2015): 279-286.
[29] Ying, D., Tian, R., Wang, X., Hang, C., Yu, F., Zhou, L. Meng, X., and Tian, Y., "Coupling effects of mechanical vibrations and thermal cycling on reliability of CCGA solder joints," M*icroelectronics Reliability* (2015).
[30] Jennings, J.M., "Comparative Analysis of CCGA Solder Column Interconnects Following Aerospace Level Vibration Testing to Failure," *Surface Mount Technology Association International Proceedings*, 2014, (website), http://www.smta.org/, accessed Nov. 15, 2015
[31] Lall, P., Kewal, P., Ryan, L., Strickland, M., Blanche, J., Geist, D., and Montgomery, R., "Modeling and Reliability Characterization of Area-Array Electronics Subjected to High-g Mechanical Shock up to 50,000 g." In *Electronic Components and Technology Conference (ECTC), 2[012 IEEE 62nd*, pp. 1194-1204. IEEE, 2012.
[32] Lall, P., Strickland, M., Geist, D., and Montgomery, R., "High-G Shock Reliability of Ceramic Area-Array Packages," *IEEE InterSociety Thermal Conference (ITherm)*, San Diego, CA May 31–June 2, 2012.
[33] Suhir, E., Ghaffarian, R., Bechou, J. and Nicolics, J., "Column-Grid-Array (CGA) Technology Could Lead to a Highly Reliable Package Design,", to be published in the *2016 IEEE Aerospace Conference Proceedings*, Big Sky Montana, March 5-12, 2016

[34] Suhir, E., Ghaffarian, R., "Predicted Stresses in a Ball-Grid-Array (BGA)/Column-Grid-Array (CGA) Assembly with a Low Modulus Solder at Its Ends." *Journal of Materials Science: Materials in Electronics*: 1-9. 2015

[35] Suhir, E., Ghaffarian, R., and Nicolics, J. "Could Thermal Stresses in A BGA/CGA-System be Evaluated From a Model Intended for a Homogeneously Bonded Assembly?" *Journal of Materials Science: Materials in Electronics*, 1-10. 2015

[36] Suhir, E., Ghaffarian, R., and Nicolics, "Predicted Stresses in a Ball-Grid-Array (BGA) and Column-Grid-Array (CGA) Interconnections in a Mirror-Like Package Design", *Journal of Materials Science: Materials in Electronics*, 2015

[37]. Suhir, E., Ghaffarian, R., "Column-Grid-Array (CGA) vs. Ball-Grid-Array (BGA) in Board-Level Drop Test: Could Stress Relief in the Solder Material Be Expected?", Journal of Materials Science: Materials in Electronics, 2016t